Session 2A6
Antennas

Synthesis of Aperture-Field Distributions for of High-Gain Phased Arrays

R. A. Speciale
Research and Development Inc., USA

Recent analytical and numerical studies of rather unusual aperture-field distributions for high-gain phased arrays have generated some interesting new results, while leading to a deeper insight, and understanding of the underlying radiation process. The planar, circular-aperture distributions analyzed were synthesized as weighted linear combinations of **TE** and **TM** cylindrical wave-modes with equal azimuth symmetry order $\boldsymbol{m}$. The **TE** and **TM** cylindrical modes used were mathematically defined as linear combinations of the W. W. Hansen's **M** and **N** basis vector-fields, using only Bessel functions of the first kind to express the radial dependence of the five **TE**, and of the five **TM** field-components. The closedform expression of the radial component $\boldsymbol{S}_R^*$ of the Complex Poynting Vector shows that the radial energyflow density of the combined **TE** and **TM** aperture-fields is identically zero, *everywhere* in the half-space above the $\mathbf{z} = 0$ plane of the aperture, for any values of the radial and azimuth coordinates $\boldsymbol{r}$ and $\boldsymbol{\varphi}$, and of the symmetry order $\boldsymbol{m}$. Further, the imaginary part of the vector product $\boldsymbol{S}_R^*$, that represents *reactive power flow* in the radial direction, also becomes identically zero, when the two mode-types are linearly combined with equal weights. At the same time, however, the axial component $\boldsymbol{S}_{\mathbf{Z}}^*$ of the Complex Poynting Vector of the combined **TE** and **TM** fields is non-zero, and is oriented along the positive z-axis, thus generating a broadside high-gain beam. It appears then that the linear combination of **TE** and **TM** cylindrical wave-modes, with equal order $\boldsymbol{m}$, results in the total cancellation of the radial, active-energy flow, *everywhere* in the $\mathbf{z} \geq 0$ radiation half-space, at all radial, azimuth, and axial positions. The results of preliminary computations, with $\boldsymbol{m} = 1$, show that the electric-field components $\mathbf{E_r}$, $\mathbf{E}_\varphi$ and $\mathbf{E_z}$ have a decaying oscillatory radial dependence, while the axial component $\boldsymbol{S}_z^*$ of the Complex Poynting Vector is sharply peaked at the center of the circular aperture. The azimuth component $\boldsymbol{S}_\varphi^*$ of the Complex Poynting Vector is zero a the center of the aperture, and has a mostly non-decaying oscillatory radial dependence. The axial ratio $\rho = \mathbf{E}_\varphi/\mathbf{E_r}$ is exactly equal to **1** on axis (at the center of the aperture), thus representing circular polarization, and goes through poles and zeros with increasing radius. The radiation pattern in the near-, Frenel, and far-field is being determined by using the Green's function, and by combining all the components of the **E** and **H** fields. Present analysis efforts aim at determining an optimum aperturetruncation radius, and an optimum radial *filtering (or windowing)*. As no rigorous procedure is as yet known for determining the optimum combination of truncation radius and radial filter shape, a rather heuristic approach is being used. It has been determined that the new, unusual aperture-distribution may be represented by a continuous spectrum of planar waves, where all the spectrum components have propagation vectors **K** oriented at a constant angle $\boldsymbol{\gamma}$ relative to the broadside z-axis, and phases that are linearly dependent on the azimuth angle $\boldsymbol{\varphi}$. As a consequence, the resulting total phase-front appears to have the shape of a circular helical-surface, similar to a corkscrew. It has been concluded that the radiated beam, generated by that distribution, appears to be the microwave equivalent of an *optical vortex*.

REFERENCES

1. Stratton, J. A., *Electromagnetic Theory*, Chapter VII, 392.

Advanced Design of Phased Array Beam-forming Networks

R. A. Speciale
Research & Development Inc, USA

Abstract—Recent fundamental results [1] in the theory of linear, multi-port networks enable cost-effective, higher-reliability designs for electronically-steered phased arrays. The referenced paper documents and proves that, by including a properly designed beam-forming network, it becomes possible to feed an array and steer its beam, using a much reduced number of expensive and critical phase- and amplitude-controlled sources, while at the same time completely eliminating the adverse effects of element coupling. Those new results are based on a generalization of the classical concepts of *scalar* image impedance, and of *scalar* image-transfer function for two-port networks, to the new concepts of multidimensional image-impedance *matrix*, and of multidimensional image-transfer function *matrix* for linear multi-port networks.

1. The Price of Performance

Electronically-steered phased arrays provide unsurpassed agility and high angular resolution in beam-pointing, and the capability of adaptive, multifunction performance. Such highly desirable features are however only attained at the price of high cost, extreme complexity, and limited reliability. Indeed, electronically-steered phased arrays are almost always designed as active-aperture system, that include a large number of semiconductor devices and beamsteering control-elements, embedded in the physical array structure, and closely connected with all the array radiating elements. The phased arrays used in radar systems use transmit/receive modules (T/R), essentially tiny radar, each nested behind a radiating element, in a half-wavelength square section of the total array aperture. Because of the well-known low power-efficiency of semiconductors, a large heat-flux is developed locally, thus generating a complex cooling problem. Finally, notwithstanding technology advances the semiconductor devices and beam-steering control-elements still are the most expensive components of electronically-steered phased array, and cost-effective designs would only be attained by reducing their total number. Those cost and reliability advantages are however only attainable if the structure of the beam-forming network used establishes a pattern of *synergistic connectivity*, where *each* controlled source simultaneously feeds *all* the array elements, and *each* array element is simultaneously fed by *all* the sources (Figures 1 and 2).

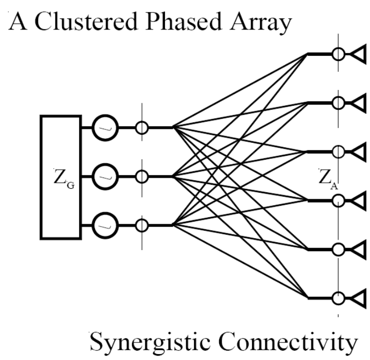

Figure 1: A clustered phased array providing synergistic connectivity.

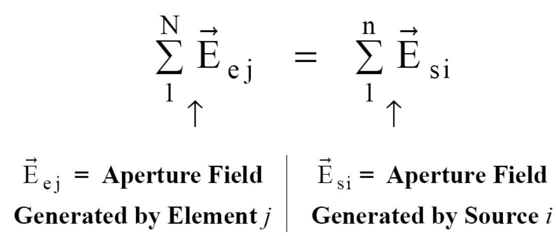

Figure 2: The aperture field is a superposition of components.

2. Non-symmetric Beam-forming Network

Such cost and complexity reductions could only be feasible by including a non-symmetric, multiport beam-forming network between the reduced number of active devices, and the much larger number of array radiating elements. Such beam-forming network would necessarily be non-symmetric, because of including an $\boldsymbol{n}$-port interface on the side of the active devices, and an $\boldsymbol{N}$-port interface on the side of the array radiating elements, with $\boldsymbol{n} < \boldsymbol{N}$ (Figures 3 and 4). The use of a reduced number of beam-steering control-elements appears possible, by considering that current active apertures have the capability of creating a very large number of completely superfluous aperture distributions, that do not generate any practical radiation pattern. Also, the angular resolution of beam-steering could be without penalty reduced, by steering the beam in increments being only a fraction of the –3 dB beam-width.

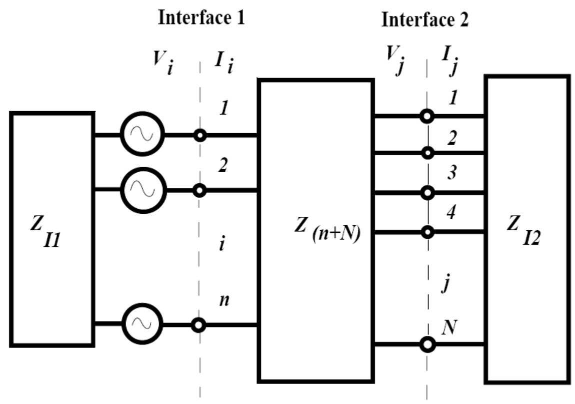

Figure 3: Unconditional, bilateral image-impedance match: forward-wave, n-phase excitation, with arbitrary wave amplitudes and phases.

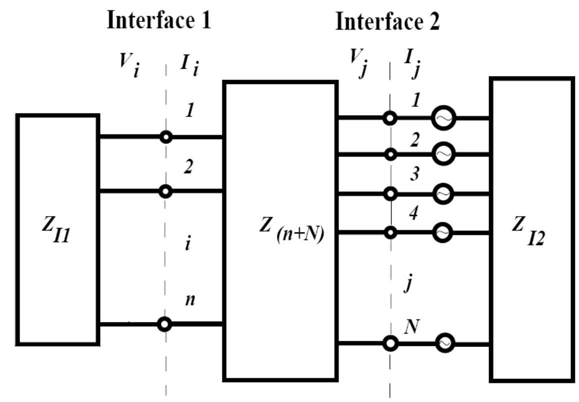

Figure 4: Unconditional, bilateral image-impedance match: backward-wave, N-phase excitation, with arbitrary wave amplitudes and phases.

3. Recent Theoretical Results

The referenced, recent fundamental results [1] in the theory of multi-port networks have been attained by introducing a generalization of the classical concept of scalar image-impedance of two-port networks, to that of image-impedance *matrices* for multiport networks. Similarly, the classical concept of scalar image-transfer function of two-port networks, has been generalized to that of image-transfer function *matrices* for multiport networks. These generalizations have made possible the design of non-symmetric beam-forming networks, that are simultaneously impedance-matched to the external environment at both interfaces, while having prescribed two-way transfer functions between two interfaces with different number of ports ($\boldsymbol{n} < \boldsymbol{N}$).

4. Image Impedance Matrices

The first fundamental new result expresses the $\boldsymbol{n} \times \boldsymbol{n}$ image-impedance matrix $\boldsymbol{Z}_{I1}$ for the $\boldsymbol{n}$-port interface-1, and the $\boldsymbol{N} \times \boldsymbol{N}$ image-impedance matrix $\boldsymbol{Z}_{I2}$ for the $\boldsymbol{N}$ -port interface-2, as functions of the four different-size blocks $\boldsymbol{Z}_i$ of the $(\boldsymbol{n}+\boldsymbol{N}) \times (\boldsymbol{n}+\boldsymbol{N})$ impedance matrix of a non-symmetric, multi-port network:

$$Z_{I1} = (I_n - Z_2 \cdot Z_4^{-1} \cdot Z_3 \cdot Z_1^{-1})^{1/2} \cdot Z_1 = (I_n - P_n)^{1/2} \cdot Z_1 \tag{1}$$

$$Z_{I2} = (I_N - Z_3 \cdot Z_1^{-1} \cdot Z_2 \cdot Z_4^{-1})^{1/2} \cdot Z_4 = (I_N - P_N)^{1/2} \cdot Z_4 \tag{2}$$

where the $\boldsymbol{n} \times \boldsymbol{n}$ matrix product $\boldsymbol{P}_n$, and the $\boldsymbol{N} \times \boldsymbol{N}$ matrix product $\boldsymbol{P}_N$ are given by:

$$P_n = M_n \cdot M_N = Z_2 \cdot Z_4^{-1} \cdot Z_3 \cdot Z_1^{-1} = M_{Pn} \cdot \Lambda_{Pn} \cdot M_{Pn}^{-1} \tag{3}$$

$$P_N = M_N \cdot M_n = Z_3 \cdot Z_1^{-1} \cdot Z_2 \cdot Z_4^{-1} = M_{PN} \cdot \Lambda_{PN} \cdot M_{PN}^{-1} \tag{4}$$

The partial matrix-products $\boldsymbol{M}_n$ and $\boldsymbol{M}_N$ in the expressions Eqs. (3) and (4) are defined as:

$$M_n = Z_2 \cdot Z_4^{-1} \tag{5}$$

$$M_N = Z_3 \cdot Z_1^{-1} \tag{6}$$

and the matrix products $\boldsymbol{P}_n$, and $\boldsymbol{P}_N$ are mutually related by the expression:

$$P_N \cdot (M_N \cdot M_{Pn}) = M_N \cdot (M_n \cdot M_N) \cdot M_{Pn} = M_N \cdot P_n \cdot M_{Pn} = (M_N \cdot M_{Pn}) \cdot \Lambda_{Pn} \tag{7}$$

By connecting external load-networks with internal impedance matrices $\boldsymbol{Z}_{L1} = \boldsymbol{Z}_{I1}$ and $\boldsymbol{Z}_{L2} = \boldsymbol{Z}_{I2}$ to the two interfaces, the two image-impedance matrices will transform to each other through the non-symmetric network:

$$Z_{I1} = Z_1 - Z_2 \cdot (Z_4 + Z_{I2})^{-1} \cdot Z_3 \tag{8}$$
$$Z_{I2} = Z_4 - Z_3 \cdot (Z_1 + Z_{I1})^{-1} \cdot Z_2 \tag{9}$$

5. The Block-traceless Scattering Matrix

Because of the bilateral impedance match so attained, the $(\boldsymbol{n}+\boldsymbol{N}) \times (\boldsymbol{n}+\boldsymbol{N})$ scattering matrix $\boldsymbol{S}$ of the nonsymmetric network becomes *block-traceless*, with only the two rectangular blocks $\boldsymbol{S}_2$ and $\boldsymbol{S}_3$ being non-zero:

$$S = \begin{vmatrix} 0 & S_2 \\ S_3 & 0 \end{vmatrix} \tag{10}$$

$$S_2 = Z_2 \cdot Z_4^{-1} \cdot \left[I_N + (I_N - Z_3 \cdot Z_1^{-1} \cdot Z_2 \cdot Z_4^{-1})^{1/2} \right]^{-1} \tag{11}$$

$$S_3 = Z_3 \cdot Z_1^{-1} \cdot \left[I_n + (I_n - Z_2 \cdot Z_4^{-1} \cdot Z_3 \cdot Z_1^{-1})^{1/2} \right]^{-1} \tag{12}$$

6. Modal and Spectral Analysis

Two other fundamental new results express the modal matrix $\boldsymbol{M}_S$, and the spectral matrix $\boldsymbol{\Lambda}_S$ of the *autonormalized* (normalized to the matrices $\boldsymbol{Z}_{I1}$ and $\boldsymbol{Z}_{I2}$), *block-traceless* $(\boldsymbol{n}+\boldsymbol{N}) \times (\boldsymbol{n}+\boldsymbol{N})$ scattering matrix $\boldsymbol{S}$ as:

$$M_S = \begin{vmatrix} M_1 & M_2 \\ M_3 & M_4 \end{vmatrix} \tag{13}$$

$$\Lambda_S = \begin{vmatrix} \Lambda_1 & 0 \\ 0 & \Lambda_4 \end{vmatrix} \tag{14}$$

The modal matrix $\boldsymbol{M}_S$ has two square diagonal blocks $\boldsymbol{M}_1$ of size $\boldsymbol{n} \times \boldsymbol{n}$, and $\boldsymbol{M}_4$ of size $\boldsymbol{N} \times \boldsymbol{N}$, and two rectangular blocks $\boldsymbol{M}_2$ of size $\boldsymbol{n} \times \boldsymbol{N}$, and $\boldsymbol{M}_3$ of size $\boldsymbol{N} \times \boldsymbol{n}$, while the blocks $\boldsymbol{\Lambda_1}$ and $\boldsymbol{\Lambda_2}$ are $\boldsymbol{n} \times \boldsymbol{n}$, and $\boldsymbol{N} \times \boldsymbol{N}$:

$$M_1 = M_{Pn} \tag{15}$$
$$M_2 = -P_n^{-1/2} \cdot Z_2 \cdot Z_4^{-1} \cdot M_{PN} \tag{16}$$
$$M_3 = Z_3 \cdot Z_1^{-1} \cdot M_{Pn} \cdot \Lambda_{Pn}^{-1/2} \tag{17}$$
$$M_4 = M_{PN} \tag{18}$$
$$\Lambda_1 = \Lambda_{Pn}^{1/2} \cdot \left[I_n + (I_n - \Lambda_{Pn})^{1/2} \right]^{-1} = Diag(e^{-\gamma_n}) \tag{19}$$
$$\Lambda_4 = -\Lambda_{PN}^{1/2} \cdot \left[I_N + (I_N - \Lambda_{PN})^{1/2} \right]^{-1} = Diag(e^{-\gamma_N}) \tag{20}$$

Most remarkably, the block $\boldsymbol{\Lambda}_4$ includes $\boldsymbol{N}-\boldsymbol{n}$ identically-zero eigenvalues, that correspond to the $\boldsymbol{N}-\boldsymbol{n}$ identically-zero eigenvalues of the spectral matrix $\boldsymbol{\Lambda}_{PN}$ of the matrix $\boldsymbol{P}_N$, while the remaining $\boldsymbol{n}$ eigenvalues are equal to those in block $\boldsymbol{\Lambda}_1$, save for a sign change. The $2\boldsymbol{n}$ non-zero eigenvalues in the spectral matrix $\boldsymbol{\Lambda}_S$, and the corresponding eigenvectors, identify the two sets of $\boldsymbol{n}$ *forward*, and $\boldsymbol{n}$ *backward, natural transmission modes* of any given non-symmetric beam-forming network, while the $\boldsymbol{N}-\boldsymbol{n}$ eigenvectors, that correspond to the zero-eigenvalues in block $\boldsymbol{\Lambda}_4$, span the *null-space* of the $\boldsymbol{n} \times \boldsymbol{N}$ block $\boldsymbol{S}_2$, and identify the *natural cut-off* modes of the network. These are the $\boldsymbol{N}-\boldsymbol{n}$ voltage-wave $\boldsymbol{a}_j$ vectors of the $\boldsymbol{N}$-port interface-2, for which the *received* $b_i = S_2 \cdot a_j$ vectors of the $\boldsymbol{n}$-port interface-1 are all identically zero.

7. The Required Impedance Matrix

The final referenced fundamental result expresses the two square blocks $\boldsymbol{Z}_1$ of size $\boldsymbol{n} \times \boldsymbol{n}$, $\boldsymbol{Z}_4$ of size $\boldsymbol{N} \times \boldsymbol{N}$, and the two rectangular blocks $\boldsymbol{Z}_2$ of size $\boldsymbol{n} \times \boldsymbol{N}$, and $\boldsymbol{Z}_3$ of size $\boldsymbol{N} \times \boldsymbol{n}$, as functions of the two required imageimpedance matrices $\boldsymbol{Z}_{I1}$ and $\boldsymbol{Z}_{I2}$, and of the two required rectangular image-transfer function matrices

$\boldsymbol{S}_2$ and $\boldsymbol{S}_3$:

$$Z_1 = (I_n - S_2 \cdot S_3)^{-1} \cdot (I_n + S_2 \cdot S_3) \cdot Z_{I1} \tag{21}$$
$$Z_2 = 2(I_n - S_2 \cdot S_3)^{-1} \cdot S_2 \cdot Z_{I2} \tag{22}$$
$$Z_3 = 2(I_N - S_3 \cdot S_2)^{-1} \cdot S_3 \cdot Z_{I1} \tag{23}$$
$$Z_4 = (I_N - S_3 \cdot S_2)^{-1} \cdot (I_N + S_3 \cdot S_2) \cdot Z_{I2} \tag{24}$$

REFERENCES

1. Speciale, R. A., "Advanced design of phased array beam-forming networks," *IEEE Antenna and Propagation Magazine*, Vol. 38, No. 4, 22–34, August 1996.
2. Speciale, R. A., "Synthesis of phased array aperture distributions," *unpublished monograph*, available for downloading from http://home.comcast.net/∼rspeciale/.
3. Speciale, R. A., "Renormalization of the scattering matrix," *Proceedings of the* 17^{th} *ACES Review*, and also available for downloading from: http://home.comcast.net/∼rspeciale/. Monterey, California, 553–561, March 19–23, 2001.
4. Speciale, R. A., "Suppression of reflections and cross-talk," *Proceedings of the* 17^{th} *Annual Review of Progress in Applied Computational Electromagnetics*, and also available for downloading from: http://home.comcast.net/∼rspeciale/. Monterey, California, 562–573, March 19–23, 2001.

Slotline Leaky Wave Antenna with a Stacked Substrate

J. Macháč, J. Hruška, and J. Zehentner
Czech Technical University, Czech Republic

Abstract—This paper presents a new version of a leaky wave antenna based on a conductor-backed slotline with a stacked substrate. The antenna radiates due to the first order space leaky wave excited on a slotline with a wide slot. The antenna radiates into the one main beam above the substrate. The main lobe of the radiation pattern is relatively wide and there is also intensive radiation in the backward direction and below the substrate. Shaping the background metal layer produces a reflector, which reduces the parasitic radiation by 7 dB. When this background layer is larger than the substrate the radiation below the substrate is additionally reduced by 3 dB. The reflector moreover reduces the width of the main beam.

1. Introduction

All kinds of open planar transmission lines are predisposed to excite leaky waves. There are two kinds of leaky waves. Surface leaky waves radiate power into the substrate. These waves are in most cases undesirable as they increase losses, cause distortion of the transmitted signal and cross-talk to other parts of the circuit. Space leaky waves radiate power into a space and mostly also into the substrate. These waves can be utilized in leaky wave antennas.

Leaky wave antennas have been known for nearly 50 years [1]. The first microstrip line leaky wave antenna was described in [2] and its behaviour was analyzed in detail in [3]. The first slotline leaky wave antenna was reported in [4]. We have investigated space leaky waves on a slotline (SL) [5] and on a conductor backed slotline (CBSL) [6]. Based on these studies we have designed, fabricated, and measured several leaky wave antennas, as, e. g., the slotline leaky wave antenna in [7]. The drawback of this antenna is radiation into two main beams, one above and one below the substrate. For this reason we turned to the CBSL. Various designed and fabricated antennas utilizing this line [8, 9] radiate only into the one main beam. This beam is rather wide with a high level of the side lobes (SLL). The antenna substrate has to be thick enough for effective radiation. From the fabrication point of view it is more convenient to use a stacked substrate. One slab is a thin commercially available substrate, while the second slab, known as the spacer, is filled with air [10].

This paper presents a slotline leaky wave antenna with a stacked substrate and conductor backing. The antenna radiates the space leaky wave of the first order. The CBSL with a wide slot and substrate consisting of two layers was analyzed by the APTL Program [11] based on the spectral domain method. The CST Microwave Studio performed optimization of an antenna feeder. The shape of the radiation pattern of the antenna has been improved by the background conductor formed into a simple reflector. This makes the main radiation lobe narrower, and considerably reduces the level of the side lobes.

2. Antenna Structure

The cross-section of the CBSL with a stacked substrate is shown in Fig. 1. The upper layer is substrate GIL1000 1.52 mm in thickness with permittivity $\varepsilon_{r2} = 3.05$, loss factor tg$\delta = 0.004$ and metallization thickness $t = 0.03$ mm. The bottom layer is air, so $\varepsilon_{r1} = 1$. Assuming that the slot is wide enough, this transmission line can support propagation of a space leaky wave of the first order with odd symmetry of the transversal component of the electric field parallel to the substrate. The dispersion characteristics of this wave calculated by the APTL Program [11] are plotted in Fig. 2. The phase constant β and the attenuation constant α are normalized to the propagation constant in free space k_0. The upper dielectric layer, in Fig. 1, has the parameters stated above, the slot width is 30 mm and three different heights of the air layer h_2=10, 15, and 20 mm were used. The simulation in Microwave Studio showed that for h_2 lower than 10 mm unwanted modes excite between the parallel plates, and the radiation efficiency is low. For values of h_2 higher than 20 mm the parasitic radiation into the space below the backed metallization increases. The value $h_2 = 20$ mm was therefore chosen as a compromise between these two limits. The dispersion characteristic of the leaky mode on the CBSL with $h_2 = 20$ mm, Fig. 2, shows that this mode can be effectively excited from 4 to 10 GHz, as its phase constant is lower than k_0 and the attenuation constant has a reasonably low value. The phase constant slowly increases

Figure 1: Cross-section of the CBSL with a stacked substrate.

with frequency. The direction of the main lobe radiation pattern, determined by the phase constant, depends therefore slightly on the frequency.

The final antenna setup is shown in Fig. 3. The antenna is fed from a coaxial cable via a CPW terminated by a patch to transform the incident energy effectively into a space leaky wave of the first order. CBSL open end termination in the form of a wedge was used. The feeder geometry was optimized in the CST Microwave Studio for minimum return losses in the widest possible frequency band when the space leaky wave is effectively excited.

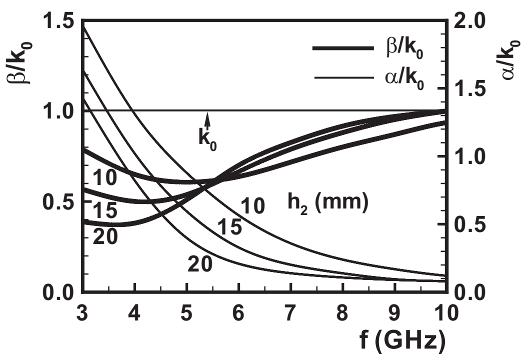

Figure 2: Normalized dispersion characteristic of the CBSL with a stacked substrate defined in the text.

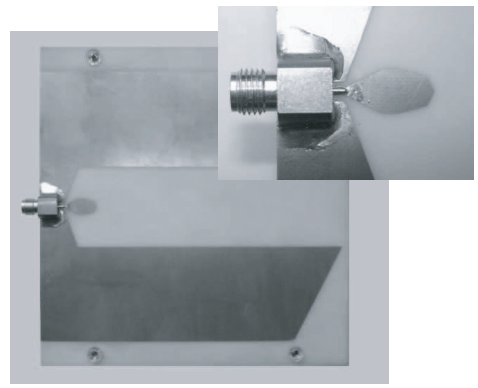

Figure 3: The fabricated antenna with the feeder shown in detail.

The resulting frequency dependence of S_{11} measured and calculated by the CST Microwave Studio is plotted in Fig. 4. The antenna is matched from 5 GHz up to 7 GHz, when $|S_{11}| < -10$ dB. The measured and calculated antenna radiation patterns at 6 and 7 GHz are plotted in Fig. 5 and are in good accord. Angle Θ is read according to Fig. 6. The radiation patterns measured at additional frequencies are plotted in Fig. 6. This antenna has only a small difference between the level of the main lobe and side lobes (side lobe level—SLL), see Fig. 8, and relatively intensive radiation under the substrate. The level of the lobes directed under the substrate is about -13 dB comparing to the main lobe. The main lobe slightly tilts in the forward direction and the full width at half power (FWHP) of the main lobe decreases with frequency, as follows from Fig. 8.

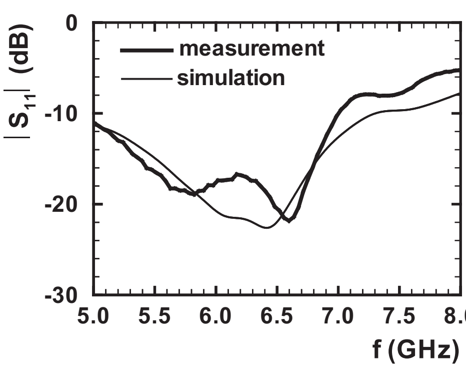

Figure 4: S_{11} of the fabricated antenna.

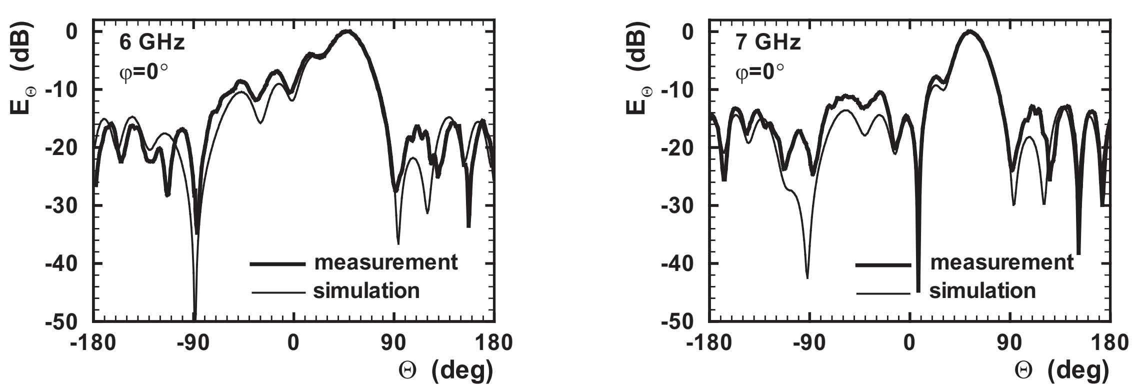

Figure 5: Radiation patterns of the antenna from Fig. 3 at 6 and 7 GHz.

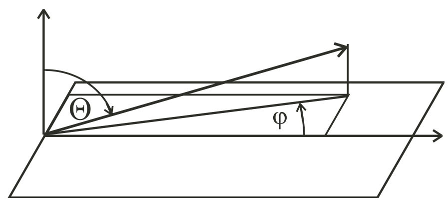

Figure 6: Orientation of angles.

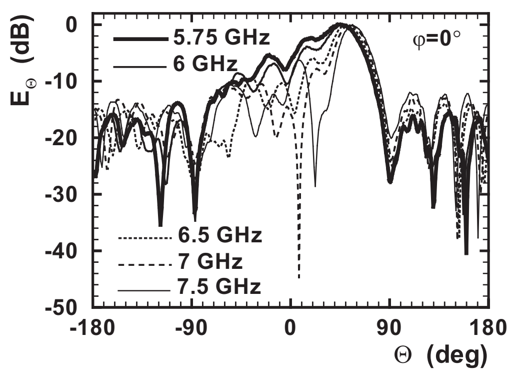

Figure 7: Radiation pattern of the antenna from Fig. 3 measured at 5.75, 6, 6.5, 7, and 7.25 GHz.

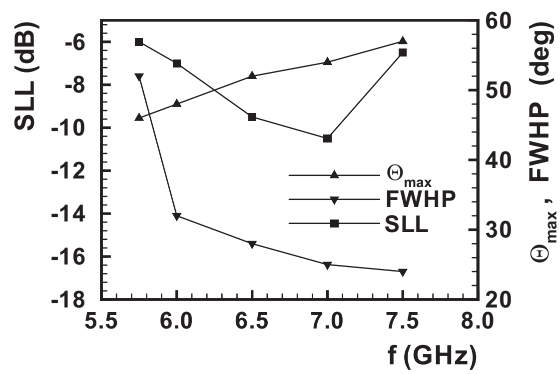

Figure 8: Measured side lobe level, full width at half power, and the angle of maximum radiation of the antenna from Fig. 3.

3. Antenna with a Reflector

The radiation pattern of the CBSL antenna with a stacked substrate has one rather wide main lobe. The antenna also radiates backward and below the backed metallization, Figs. 5, 7 and 8. Its radiation pattern can be shaped effectively by adding the background metal reflector [10], Fig. 9. The layout of the feeder and of the slotwidth was left without any change. This antenna was simulated by CST Microwave Studio with the aim to reduce the side lobes with a reasonably small reflector. Finally the reflector position is 20 mm behind the substrate edge and exceeds the substrate height by 20 mm. This reflector scarcely influences the antenna input impedance. Fig. 10 compares the measured and calculated radiation patterns of the antenna with the reflector at 7 GHz. The radiation patterns measured at three different frequencies are plotted in Fig. 11. Comparing the radiation patterns in Fig. 11 and Fig. 7, we see that the antenna with the reflector has a narrower main beam and the level of both the side lobes and of the lobes directed under the substrate are reduced by 7 dB.

Making the size of the background metal layer larger than the antenna substrate further reduces the radiation below the substrate. In this way we get the antenna shown in Fig. 12. The reflector has the same geometry as in Fig. 9, the bottom conductor is enlarged by 30 mm on the side and front walls of the substrate.

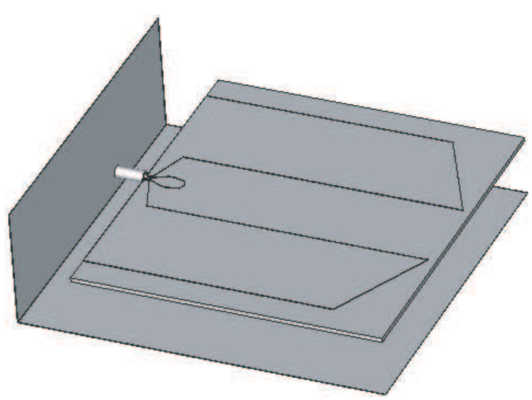

Figure 9: The Microwave Studio model of the antenna with a reflector.

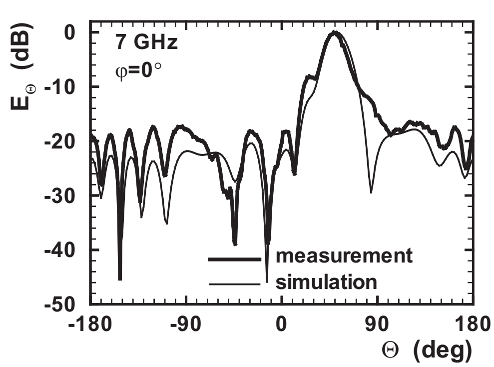

Figure 10: Radiation pattern of the antenna from Fig. 9 at 7 GHz.

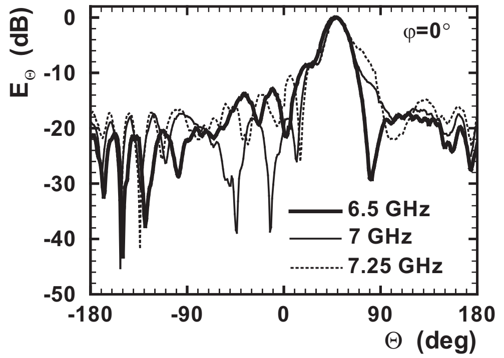

Figure 11: Radiation pattern of the antenna from Fig. 9 measured at 6.5, 7 and 7.25 GHz.

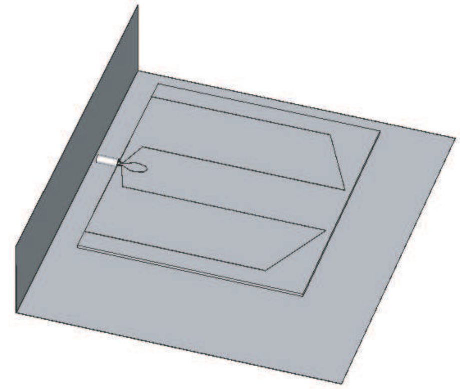

Figure 12: The Microwave Studio model of the antenna with a reflector and the background metal layer larger than the substrate by 30 mm.

The measured and calculated radiation patterns of this antenna are plotted in Fig. 13 at the frequency 6.75 GHz. The two lines fit each other well. The radiation patterns of this antenna measured at several frequencies are plotted in Fig. 14. It follows from Figs. 13 and 14 that the radiation below the substrate is reduced by 3 dB comparing to the antenna from Fig. 9 and by 10 dB comparing to the original antenna without the reflector in Fig. 3. The SLL is reduced from 6.5 to 6.75 GHz to -17 dB. The FWHP of the main beam varies around 20 deg when the frequency changes, which is considerably lower than the FWHP of the antenna from Fig. 3. The direction of the main lobe is saved. The SLL, FWHP, and the angle of maximum radiation of the antenna from Fig. 12 are plotted in Fig. 15. The plot in Fig. 15 in comparison with the plot in Fig. 8 shows the improvement of the radiation pattern when the reflector is applied.

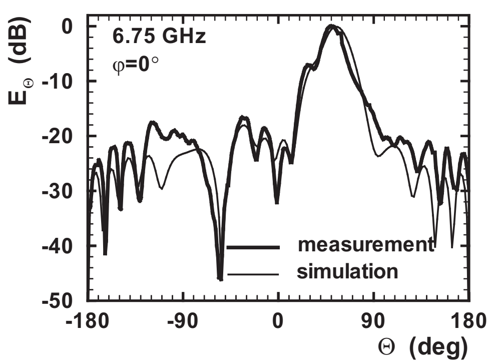

Figure 13: Radiation pattern of the antenna from Fig. 12 at 6.75 GHz.

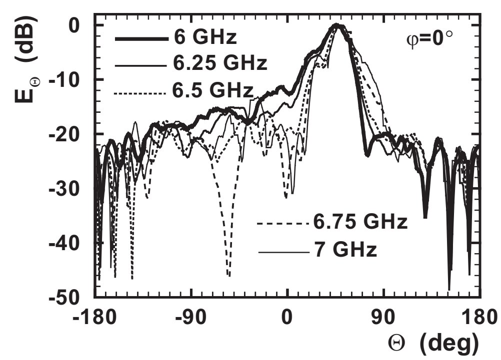

Figure 14: Radiation pattern of the antenna from Fig. 12 measured at 6, 6.25, 6.5, 6.75 and 7 GHz.

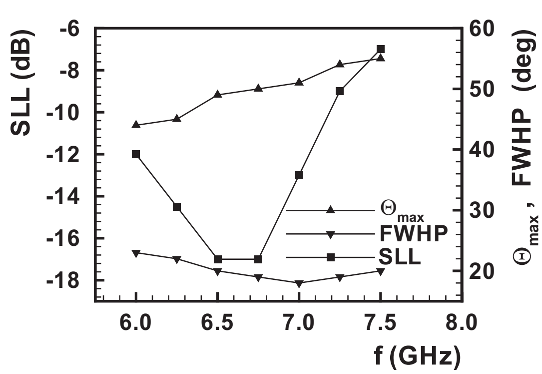

Figure 15: Measured side lobe level, full width at half power, and the angle of maximum radiation of the antenna from Fig. 12.

4. Conclusion

This paper presents a leaky wave antenna based on a conducto-backed slotline with a stacked substrate. This substrate consists of a thin dielectric layer and a thick air spacer. The antenna radiates a first order space leaky wave with odd symmetry only into one main beam above the substrate. This beam is tilted in the forward direction when the frequency increases. The antenna layout was optimized using the CST Microwave Studio. The antenna effectively radiates from 5 to 7 GHz. Its radiation pattern has a single main beam and the side lobes are at a level not worse than -10 dB below the maximum radiation. The radiation below the substrate is not worse than -14 dB below the maximum of the main lobe.

The additional reflector effectively shaped the radiation pattern. Two versions of the antenna with the reflector were designed with the aid of the CST Microwave Studio and then fabricated and measured. The antenna feeder and the slot layout were the same as the antenna without the reflector had. The antenna with the reflector and the ground conductor of the same size as the substrate reduces the level of the side lobes to -17 dB, and the radiation below the substrate to -20 dB. The antenna with the background conductor larger than the substrate has a level of radiation below the substrate lower by an additional 3 dB, i. e., -23 dB. The width of the main lobe is around 20 deg, which is narrower than for the antenna without the reflector. The direction of this lobe is the same for the antenna both with and without the reflector.

Acknowledgement

This work has been supported by the Grant Agency of the Czech Republic under the project 102/03/0449 "New circuit devices for communication technology".

REFERENCES

1. Zurker, F. J., "Surface and leaky-wave antennas," *Antenna Engineering Handbook*, H. Jasik, ed., McGrew Hill, New York, 1961.
2. Menzel, W., "A new traveling wave antenna in microstrip," *AEÜ*, Vol. 33, 137–140, 1979.
3. Oliner, A. A., "Leakage from higher order modes on microstrip line with application to antennas," *Radio Science*, Vol. 22, No. 6, 907–912, 1987.
4. Sheen, J.-W., Y.-D. Lin, "Propagation characteristics of the slotline first higher order mode," *IEEE Trans. Microwave Theory Techn.*, Vol. MTT-46, No. 11, 1774–1781, 1998.
5. Zehentner, J., J. Machac, P. Lorenz, "Space leakage of power from the slotline," *2001 IEEE MTT-S IMS Digest*, Phoenix, AZ, Vol. 2, 1217–1220, 2001.
6. Zehentner, J., J. Machac, J. Mrkvica, C. Tuzi, "The inverted conductor-backed slotline—a challenge to antenna and circuit design," *33rd European Microwave Conference*, Munich, Germany, Proceedings Vol. 1, 73–76, 2003.
7. Zehentner, J., J. Machac, P. Lorenz, J. J. Mrkvica, "Planar slot-patch antenna," *31st European Microwave Conference*, London, UK, Proceedings Vol. 3, 223–226, 2001.
8. Machac, J., J. Zehentner, "Radiation from the conductor-backed slotline," *2004 URSI International Symposium on Electromagnetic Theory*, Pisa, Italy, Proceedings Vol. 1, 162–164, 2004.
9. Machac, J., J. Zehentner, J. Hruska, "Conductor-backed slotline antenna," *34th European Microwave Conference*, Amsterdam, Netherlands, Proceedings Vol. 2, 1205–1208, 2004.
10. Hruska, J., "Slotline antenna with a leaky wave," *Diploma Thesis*, (in Czech), Czech Technical University, 2005.
11. Zehentner, J., J. Mrkvica, J. Machac, "Analysis and design of open planar transmission lines," *East-West Workshop Advanced Techniques in Electromagnetic*, Warszawa, Poland, 2004.

Coplanar Multi-line Antenna Design for Thin Wireless Terminal

K. Takei, **Y. Shirakawa**, **and M. Ikegaya**
Hitachi Cable Ltd., Japan

To improve portability of wireless apparatus, recently their shapes have been required thinner and thinner. On the other hand, responding starts of several kinds of multi-media wireless services, ex. wireless LAN (WLAN), 2.5/3 G cellar phone, terrestrial digital TV and etc., it is necessary to provide multi-mode antennas. The coplanar line antenna (CPLA), which consists of finite a self ground and strip lines around it, is suitable for thin shape multi-mode antenna [1]. This antenna has been widely used as multi-mode WLAN antenna for mainly notebook PC application. CPLA can be designed using simple modified transmission line theory, which is obtained by replacing conventional line with new line having a complex transmission constant due to radiation loss [2]. For the purpose of applying CPLA to smaller and thinner wireless apparatus, i.e., handy phone, PDA, and pocket PC, we propose the coplanar multi-line antenna (CPMLA), which has multi-stacked strip lines around the self ground.

To realize CPMLA in the limited small space of smaller and thinner terminal, we must analyze more precise antenna pattern, which is made under 0.5–1 mm line and space rule in stead of 2–4 mm rule of conventional CPLA. Direct EM analysis by using numerical method, i.e., FEM, FDTD, and Method of Moment, consumes huge computational time. An antenna design with computer is equal to searching out the candidate structure by using suitable searching algorithm and fast EM calculation required too many times in its algorithm. To realize the actual computer design of CPMLA, we have developed a novel design method by using the modified transmission line theory.

The novel design method is based on conventional design method of coupling transmission lines. Since strip lines of CPMLA are arranged on one ideal plane, we approximately consider only a multiple coupling between neighbor two strip lines. Different relative locations of these lines cause different self impedance of them. Because the conventional method assumes the same self impedance and the same mutual impedance caused of the coupling between neighbor lines, the scattering matrix of a multi-line structure is derived analytically. To obtain a scattering matrix of a multi-line structure with different self impedances, we have developed a recursive algorithm for such a scattering matrix as follows.

$$\overline{Z} = \begin{bmatrix} \alpha_1 & \beta & 0 & 0 \\ \beta & \alpha_2 & \ddots & 0 \\ 0 & \ddots & \ddots & \beta \\ 0 & 0 & \beta & \alpha_N \end{bmatrix}, \begin{vmatrix} \alpha_1 - \lambda_i & \beta & 0 & 0 \\ \beta & \alpha_2 - \lambda_i & \ddots & 0 \\ 0 & \ddots & \ddots & \beta \\ 0 & 0 & \beta & \alpha_N - \lambda_i \end{vmatrix} = 0, \quad \begin{matrix} \alpha_1 x_1^i + \beta x_2^i = \lambda_i x_1^i \\ \beta x_1^i + \alpha_2 x_2^i + \beta x_3^i = \lambda_i x_2^i \\ \vdots \\ \beta x_{N-1}^i + \alpha_N x_N^i = \lambda_i x_N^i \end{matrix}$$

$$\overline{Z} = {}^t\,\overline{T}\,\overline{S}\,\overline{T} = \begin{bmatrix} x_1^1 & \cdots & x_N^1 \\ \vdots & \vdots & \vdots \\ x_1^N & \cdots & x_N^N \end{bmatrix} \begin{bmatrix} z_1 & 0 & 0 \\ 0 & \ddots & 0 \\ 0 & 0 & z_N \end{bmatrix} \begin{bmatrix} x_1^1 & \cdots & x_1^N \\ \vdots & \cdots & \vdots \\ x_N^1 & \cdots & x_N^N \end{bmatrix}$$

The final equation shows that impedance matrix Z is converted into diagonal scattering matrix S. Therefore, dividing CPMLA structure along longitudinal direction of the strip line into a short period without discontinuity along this direction, EM performances can be calculated by the modified transmission line theory. Moreover, connecting each short period with the cascade matrix of conventional circuit theory according to the CPMLA topology, we can design a multi-mode antenna, ex. 800/1500/1900 MHz 3-mode antenna sized of $40 \times 50 \times 0.03$ mm.

REFERENCES

1. Japanese patent application 2001-085484.
2. Japanese patent application 2004-305873.

Effect of Distant Scatterers on MIMO Fading Channel Tracking

N. M. Khan and R. Ramer
University of New South Wales, Australia

This paper considers the problem of a wireless multi-input multi-output (MIMO) fading channel tracking, when a strong distant scattering cluster is present in the area in addition to the local scattering zone around the mobile. Time-varying fading channels are dynamic in nature and their tap values in signal processing depend significantly on the distribution of the angle of arrival (AOA) $p(\psi)$ at the mobile station. We assume N_T-input, N_R-ouput MIMO communication system where each receiver antenna observes a linear combination of all transmitted data sequences, each distorted by ISI, under white Gaussian noise [1]. Using state-space approach, a MIMO system operating over time-varying channel, can be modeled as, [1, 2].

$$h_l^{(m,j)}(i+1) = \alpha_l^{(m,j)} h_l^{(m,j)}(i) + v_l^{(m,j)}(i+1) \tag{1}$$

$$r^{(j)}(i) = \sum_{m=1}^{N_T} \sum_{l=1}^{L^{(m,j)}} h_l^{(m,j)}(i) x^{(m)}(i-l) + n^{(j)}(i) \tag{2}$$

where $h_l^{(m,j)}(i)$ is the lth tap of the impulse response of order $L^{(m,j)}$ between the mth input $x^{(m)}(i)$ (with $m = 1, \ldots, N_T$), and the jth ouput $r^{(j)}(i)$ (with $j = 1, \ldots, N_R$), of the time-varying MIMO channel, at time instant i. $x^{(m)}(i)$ is the transmitted signal from transmitter m, and $r^{(j)}(i)$ is the received signal at receiver j. $v_l^{(m,j)}(i)$ and $n^{(j)}(i)$ are i.i.d. process and measurement noises and $\alpha_l^{(m,j)}$ is the autoregressive (AR) coefficient of lth tap and accounts for the variations in the channel due to spatially dispersed multipath signals affected by the maximum Doppler shift $f_D^{(l)}$ [1–3].

$$\alpha_l = E\{h_l(i) h_l^*(i-1)\} = \int_{-\pi}^{\pi} p(\psi) e^{-j2\pi f_D^{(l)} T \cos(\psi)} d\psi \tag{3}$$

where T is the symbol duration. In rural or sub-urban areas, when mobile travels at fast speed under the influence of a dominant distant scatterer (e.g., hill), the distribution of the AOA, $p(\psi)$ deviates from the uniform shape (a common assumption usually made to find correlation statistics [1–3]), and can be written as,

$$p(\psi) = \Omega \frac{R^2 + 4D\cos(\psi - \psi_D)\sqrt{R^2 - D^2 \sin^2(\psi - \psi_D)}}{\pi R^2} \tag{4}$$

where R is the radius of the distant scattering cluster, D is the distance of its center from the mobile, ψ_D is the angle it makes with the virtual line of sight at mobile and Ω is the normalizing constant.

A variety of models may be used with different values of D, R and ψ_D depending on the terrain and geography of the area to obtain α_l, which can then be exploited in fading channel tracking algorithms using (1) and (2).

REFERENCES

1. Komninakis, C., C. Fragouli, A. H. Sayed, and R. D. Wesel, “Multi-input multi-output fading channel tracking and equalization using Kalman estimation,” *IEEE Trans. Signal Proc.*, Vol. 50, No. 5, 1065–1076, May 2002.
2. Khan, N. M. and P. B. Rapajic, “Use of state-space approach and Kalman filter estimation in channel modeling for multiuser detection in time-varying environment,” in *Proc. Intl. Workshop Ultra-Wideband Sys.*, No. 1052, Finland, June 2003.
3. Jakes, W. C., *Microwave Mobile Communications*, John Wiley, New York, 1974.

Planar Small Antenna Module for Global Positioning System

T. Ogawa and K. Takei
Hitachi Cable Ltd., Japan

Prototype of a novel planar antenna module for Global Positioning System (GPS) is developed. The antenna module consists of a circularly polarized antenna and two stages of low noise amplifiers. The size of this module is $28\,\mathrm{mm}\times 15\,\mathrm{mm}\times 2\,\mathrm{mm}$. The module works in 3 V voltage operation. The module is small, thin and lightweight, which is suitable for mobile navigation equipments.

The circularly polarized antenna receives 1575 MHz right-handed circularly polarized wave which is used on GPS. The antenna consists of two layered metal patterns. These layers are connected each other by via hole. The metal pattern is formed on both sides of one PCB. Electrical size of the antenna is about $\lambda/8$ square. Our antenna is quite smaller than a conventional ceramic patch antenna commonly used for GPS equipments of $\lambda/2$ square size. The smaller size of this antenna enables to use conventional PCB with high dielectric constant ($\varepsilon r = 10$) instead of relatively expensive ceramic block. Actual antenna size is about 12 mm square.

The antenna consists of a lot of rectangular small metal segments. We analyzed induced currents on each segment using method of moment to calculate axial ratio and input impedance of the antenna. We defined two directional currents I_v and I_h, which are perpendicular to each other, on each segment. The axial ratio (AR) is calculated as shown in equation (1). The axial ratio of designed antenna is about 2.5 dB (less than 3 dB). Therefore this antenna can receive GPS signal successfully in spite of small electrical size.

$$|AR| = \left|\frac{|I_L| + |I_R|}{|I_L| - |I_R|}\right| \quad I_L = I_V + I_H\angle 90^\circ \quad I_R = I_V\angle 90^\circ + I_H \quad I_V = \Sigma I_v \quad I_H = \Sigma I_h \tag{1}$$

The antenna and the low noise amplifier are formed on PCB. The two layered antenna is formed on both sides of PCB. Circuit pattern of two stages amplifiers is formed on one side, and ground plane is formed on the other side. On calculation of the axial ratio, we considered currents, which are induced on the antenna and the ground plane.

High gain design of first stage amplifier causes capacitive input impedance ($200 - j100\,\Omega$) of FET. Therefore, we designed antenna impedance about $200 + j100\,\Omega$ to achieve conjugate matching. The impedance of the conventional $\lambda/2$ patch antenna is about $50\,\Omega$. However, the input impedance of the low noise amplifier is not $50\,\Omega$. Therefore conventional design method requires large scale matching circuit with distributed lines. Our design method successfully omits such large scale matching circuit because it is possible to design antenna impedance and axial ratio simultaneously. We chose bipolar transistor at second stage of the amplifier to achieve output impedance around $50\,\Omega$. Hence the module can be connected to conventional demodulator directly.

REFERENCES

1. *Japanese Patent Application 2001-085484*.
2. Takei, K., *Proc. PIERS*, 154, Singapore, 2003.
3. Takei, K., et al., *Proc. China-Japan Joint Meeting on Microwaves*, 166–169, Harbin, 2004.
4. Takei, K. and T. ogawa, *Proc. ICECom*, Dubrovnik, Croatia, 2005.

Interaction of Electromagnetic Field from Cellular Base Station Antennas on Cardiac Pacemakers

R. Kubacki[1], **M. Wnuk**[2], **and J. Sobiech**[1]

[1]Military Institute of Hygiene and Epidemiology, Poland
[2]Military University of Technology, Poland

Background. The aim of this study was to investigate the possible interaction of pulsed elec-tromagnetic (EM) fields affecting the cardiac pacemakers. Pulse modulated fields typical for cellular GSM system have been considered for this study. In the literature, only interaction of electromagnetic field emitted from cellular handsets to pacemakers has been described. It has been proved that this kind of radiation is rather "safe" for pacing process. Only in same lit-erature a minimum safety distance of few centimeters from handset to the patient body was suggested. Nevertheless, no one assesses the threshold of electric field strength when pacemakers change the shape of emitted pulses or even when they inhibit of the pacing process. This is because measurements of electric field in the vicinity of handset is difficult and there is a need to assess all components of electric field vector. However, there is no information about possible interaction of radiation emitted from base station antennas on pacemaker functions. This information whether electromagnetic field from base stations can be danger for pace-makers is important for people dwelling in the vicinity of these antennas.

Our intention was to recognize whether the radiation from GSM base stations can affect pacemaker functions. All investigations were carried out in the anechoic chamber where the level of exposure and type of polarization can be precisely determined.

Methods. The base station panel antenna (Kathrein antenna type 738573) has been chosen as a source of EM field. The antenna has been fed from external generator and amplifier allowing to expose of pacemakers to EM field up to $300\,\mathrm{W/m^2}$. Microwaves (940 MHz) have been modulated with $577\,\mu$sec pulses and 867 Hz repetition frequency - every second time slot was fulfilled. In this case EM field is a pulse modulation function comparable to field emitted from base station antennas when base station is linked with 4 persons. Each pacemaker was situated in anechoic chamber with 3 typical orientation (polarization) regarding to the electric vector of the incident field. To find the susceptibility threshold to electromagnetic interference all ori-entations of pacemakers were sought to find the critical polarization of electric field.

Results. Pacemakers signals have been analyzed in function of power density of incident mi-crowaves and the following changes in pacemaker signals have been studied:

-changes of the amplitude and shape of pulses,
-changes of the repetition frequency of the pulses
-falling out of one or few pulses,
-the inhibition of the pacing process.

Values of electric field strength when the above changes occurred were found. Nevertheless, it should be underlined that the above changes occurred in strong electromagnetic field and they are dependent of the type of pacemakers and polarization of the electric field.

Computer-Simulation of Near-Field Phased-Array Radiation-Pattern Scanning

R. A. Speciale
Research and Development Inc., USA

The recently introduced Tilted-Ellipse Representation of Standing-Wave Patterns [1, 2] provides a fast and inexpensive way for extracting the multi-dimensional, complex scattering-matrices of very large, multi-port microwave systems, by performing computer-simulations of large-scale experimental-measurements, that would require a very complex and expensive multiport Automated Vector Network Analyzer, and a long data-acquisition time. That simulation method is based on the results of a rigorous mathematical analysis [1, 2] of the simultaneous propagation of forward- and backward-waves along virtual measurement lines, connected to the ports of the microwave systems being simulated. That analysis has shown that the mutual correlation between the imaginary components, and the real components of the standing-wave fields, along the length of each virtual measurementline, can be quantitatively represented by the parametric equations of a tilted-ellipse, centered on the origin of a Cartesian frame. Clearly, very significant time- and cost-savings are attained by simulating complex S-matrix experimental-measurements, when the system under simulated test has a very large number of ports ($n \gg 4$), and/or a very large number of propagating modes. Most remarkably, measurement-simulations may be performed at early stages of system design, as no prototype is required. The S-matrix measurement-simulation method described in [1, 2] makes even possible the HPC-simulation of the multi-dimensional scattering-matrix measurements required to perform near-field scans of the radiation-pattern of electronically-steered phased-array (Figure 1).

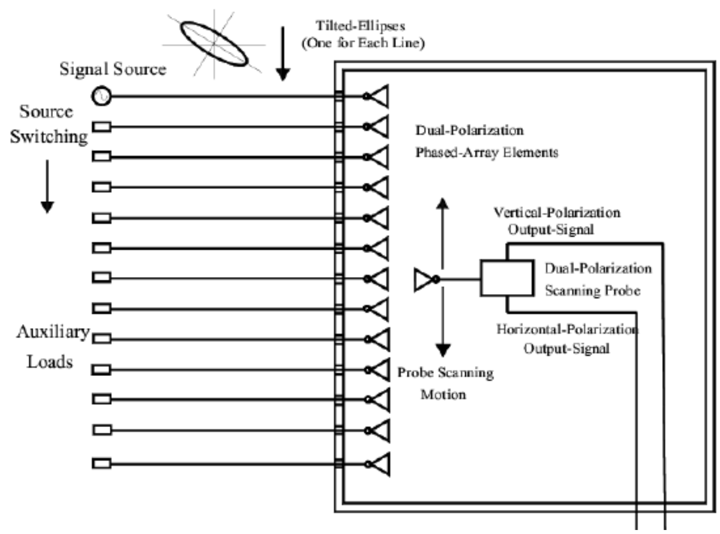

Figure 1: Phased-array in a near-field scanner.

The tilted-ellipse representation of the standing-wave patterns along each virtual line, may be used to compute the magnitudes and the phases of the forward-wave and backward-wave vectors, at any arbitrary point along all the virtual measurement-lines. The mathematical results of the previously-reported analysis of the simultaneous propagation of the forward and backward waves [1, 2], express the complex values of the forward-wave vectors, and of the backward-wave vectors, as functions of the distance from each system port, by using the semi-axes $\boldsymbol{a}$ and $\boldsymbol{b}$ of the ellipse, and the tilt-angle δ of its major axis. The new measurement-simulation performs therefore the very same wave-extraction function that, in an actual experimental measurement-session, would require the use of many Vector-Reflectometers, each composed of two directional couplers, and of a vector-voltmeter.

REFERENCES

1. Speciale, R. A., "Computing the scattering matrix of multiport systems," *PIERS 2004*, Pisa, Italy, 2004.
2. Speciale, R. A., "The tilted-ellipse representation of standing-wave patterns," *ACES 2004*, Syracuse, NY, 2004.

Dual Frequency Rectangular Microstrip Patch Antenna with Novel Defected Ground Structure

J. Sun, E.-P. Li, and Y.-J. Zhang
Institute of High Performance Computing, Singapore

Frequency operated microstrip antenna have already attracted much attention due to the practical application in communication systems. There are normally two ways to generate two operating frequency: using multi-resonator and using reactive load on the antenna structure. The reactive element can be lump element or just special structure, e. g., short pins or slot etched on the patch. By proper design, the slot will not modify the desired mode but perturb the undesired mode. Some researchers have realized more sophisticated slot design, i. e., meander shape slot on the both edge of the patch to further reduce the patch size [1]. More recently, the photonic bandgap structure has draw great attention on the electromagnetic engineering. The photonic bandgap concept (PBG) applied in electromagnetic engineering could be referred to as electromagnetic bandgap (EBG). Since the basic concept is the same and only different frequency range is involved, we could still use the term PBG to refer to the EBG related structure. It is interesting that some researchers has used the PBG structure on the ground plane to suppress the high order harmonics for the microstrip patch antenna [2], others use the PBG structure on the ground plan of the PCB board to enhance the signal integrity, i.e., to reduce the cross talk or to increase the signal to noise ratio. In this paper, we study the rectangular patch antenna with defected ground structure (DGS). This DGS structure in the ground plane is only under the feeding miscrostrip line and does not present under the microstrip patch, so that the radiation through the ground plane can be controlled to a low level. The DGS consists of three tapered photonic bandgap structure in parallel, which is similar to the design of low pass filters in [3], however, only half of the tapered photonic bandgap structure is used for our purpose. The microstrip patch antenna with DGS under the feeding stripline is shown in Fig. fig:1, where $r_1 = 1.5\,\text{mm}$, $r_2 = 1.2\,\text{mm}$, $r_3 = 1.0\,\text{mm}$, $r_4 = 0.8\,\text{mm}$, $p_1 = 3.5\,\text{mm}$, $p_2 = 4.5\,\text{mm}$, $W = 12.45\,\text{mm}$, $L = 16\,\text{mm}$. A commercially available package, CST Microwave Studio, is used to simulate the return loss using the 3-D FDTD method. Adaptive meshing scheme is adopted to obtain convergence results. The return loss for the conventional stripline feed microstrip patch antenna and our proposed structure is shown in Fig. 2. It is very interesting to note that the novel structure has two effects on the behaviour of the return loss. First, the high frequency harmonics were greatly suppressed; second, a dual frequency operation mode (the frequency ration is around 1.3) is presented. By tuning the PBG structure parameters, the second operating frequency can be shifted lower or higher in certain range.

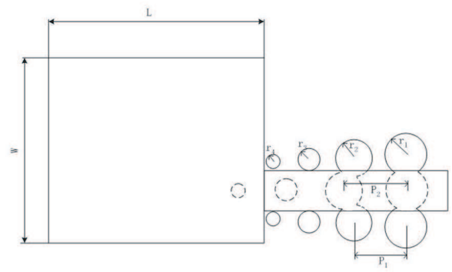

Figure 1: A microstrip patch antenna on a PBG defected ground plane.

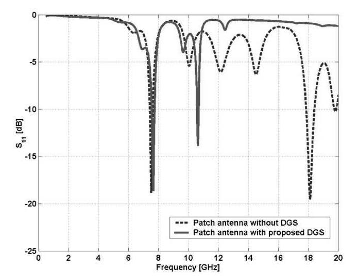

Figure 2: Return loss for the conventional microstrip antenna and proposed antenna.

REFERENCES

1. Gao, S.-C., L.-W. Li, T.-S. Yeo, and M.-S. Leong, "FDTD analysis of a slot-loaded meandered rectangular patch antenna for dual-frequency operation," *IEE Proc. -Microw. Antennas Propq.,* Vol. 148, No. 1, 65–71, 2001.
2. Liu, H., Z. Li, X. Sun, and J. Mao, "Harmonic suppression with photonic bandgap and defected ground structure for a microstrip patch antenna," *IEEE Microwave and Wireless Components Letters,* Vol. 15, 55–56, 2005.
3. Bozzetti, M., A. D'Orazio, M. DeSario, V. Petruzzelli, F. Prudenzano, and F. Renna, "Tapered photonic bandgap microstrip lowpass filters: design andrealisation," *IEE Proc. -Microw. Antennas Propq.,* Vol. 150, No. 6, 459–462, 2003.

Modeling of High Power Broadband THz Antennas

A. S. Podgorski, **J. T. MacGillivray**, **and W. D. Prather**
Air Force Research Laboratory, USA

The term THz is currently applied to electromagnetic spectrum contained between 100 GHz and 10 THz. This region of electromagnetic spectrum remains virtually unused, despite many advantages that it could provide in the area of imaging and communication. During the last 25 years the only usage of the THz spectrum was attributed to narrow-band molecular spectroscopy for Earth, planetary and space sciences. What hampered the developments in the THz area was the lack of commercially available instrumentation.

The uniqueness of the THz technology is related to the fact that, as well as providing the information on structural images of objects it could also be used for spectroscopy—to provide information on materials. At the molecular level, the biologists will have a valuable new tool as the rotations and vibrations of the DNA molecules lie in the THz range.

Current developments of THz technology fall into two categories: active and passive. Active THz technology involves firing THz-rays at an object and analyzing the radiation transmitted and reflected back. However, all objects at normal temperatures are constantly emitting relatively low levels of THz-rays, which can be detected with sensitive instruments. Because of the low level of the detected signals, the passive THz systems have to be narrowband, but the active THz systems do not need to be restricted to the narrowband. Therefore, we can expect that the future system might be active and passive, and they can be narrowband as well as broadband.

Anticipating that by extending the frequency range into the THz region the substantial losses can occur in the antenna, which is generally the longest part of the broadband generating system, we decided to concentrate the effort on modeling the antenna using the FDTD code. Although the plan is to reach 10 THz, the first broadband antenna was designed to operate in the 100 GHz to 1 THz frequency range only. The antenna was designed to ensure gain of 50 dB and output peak power level of 0.1 MW. The design of the antenna was based on a TEM-Horn Antenna that operated successfully up to 100 GHz.

Our estimate indicates that the FDTD modeling of BGF antennas operating in the 100 GHz to 1 THz, will require approximately $10,000 \times 500 \times 400$ cells and as such it could only be done using super-computers. To allow easy implementation of the antenna model into the FDTD Code, while using super-computer, four different versions of a 3-D model of the broadband antenna were prepared and considered.

The publication will present the results of this very extensive modeling effort.